Nanomed Res J 10(2):189-201, Spring 2025

RESEARCH ARTICLE

Green Synthesis of Silver and Cerium Co-Doped Zinc Oxide Nanoparticles Using Ziziphora tenuior L. Extract: Characterization and In Vitro Anticancer Activity Against Glioblastoma

Maryam Shojaee[1#], Seyed Sajad Ahmadi[2#], Omid Bagherzadeh[2#], Maryam Hatamibardar[3#], Maryam Poursharif[4], Sina Alimohammadi[4], Mohammad Jalili-Nik[1*], Seyedeh Mozhdeh Mirzaei[5*], Afsane Bahrami[6,7*]

[1] *Department of Clinical Biochemistry, Faculty of Medicine, Mashhad University of Medical Sciences, Mashhad, Iran*

[2] *Department of Ophthalmology, Khatam-Ol-Anbia Hospital, Mashhad University of Medical Sciences, Mashhad, Iran*

[3] *Student Research Committee, Babol University of Medical Sciences, Babol, Iran*

[4] *Faculty of Medicine, Mashhad University of Medical Sciences, Mashhad, Iran*

[5] *Department of Medical Biotechnology and Nanotechnology, Faculty of Medicine, Mashhad University of Medical Sciences, Mashhad, Iran*

[6] *Clinical Research Development Unit of Akbar Hospital, Faculty of Medicine, Mashhad University of Medical Sciences, Mashhad, Iran*

[7] *Clinical Research Development Unit, Imam Reza Hospital, Faculty of Medicine, Mashhad University of Medical Sciences, Mashhad, Iran*

 # Equally contributed as first authors

** Corresponding authors*

ARTICLE INFO

Article History:
Received 02 Mar 2025
Accepted 24 Apr 2025
Published 01 Jun 2025

Keywords:
Silver nanoparticles
Cerium nanoparticles
Zinc oxide nanoparticles
Ziziphora tenuior L.
Glioblastoma
Green synthesis
Co-doped

ABSTRACT

Glioblastoma multiforme (GBM) presents significant treatment challenges due to genetic heterogeneity and resistance to conventional therapies. This research investigates the prospects of green synthesized zinc oxide nanoparticles co-doped with cerium and silver (Ce-Ag@ZnO) coated by *Ziziphora tenuior* extract as an innovative anticancer agent against GBM. The results of characterizing nanoparticles by UV-Vis, FTIR, and XRD confirm the successful development of pure Ce-Ag@ZnO with a crystalline structure. The FESEM and EDX/mapping outcomes showed Ce-Ag@ZnO were spherical with a mean size of 31.77 ± 3.7 nm. These nanoparticles exhibited high selectivity toward cancer cells (U87 and U251 cell lines) with IC_{50} values of 40.56 and 45.44 µg/mL and reduced toxicity towards normal human fibroblast cells (HFF cell lines). In addition, the release of Zn^{2+} ions and the consequent increase in reactive oxygen species (ROS) production lead to apoptosis as evidenced by elevated levels of apoptotic cells. While this study presents promising insights into the anticancer efficacy and selectivity of Ce-Ag@ZnO against GBM, further research is required to investigate and clarify the intricate molecular mechanisms involved. Overall, this approach highlights the capability of nanotechnology and plant-derived compounds in developing effective therapies for resistant cancers, thereby enhancing clinical outcomes for GBM patients.

How to cite this article
Shojaee M., Ahmadi SS., Bagherzadeh O., Hatamibardar M., Poursharif M., Alimohammadi S., Jalili-Nik M., Mirzaei SM., Bahrami A. Green Synthesis of Silver and Cerium Co-Doped Zinc Oxide Nanoparticles Using Ziziphora tenuior L. Extract: Characterization and In Vitro Anticancer Activity Against Glioblastoma. Nanomed Res J, 2025; 10(2): 189-201. DOI: 10.22034/nmrj.2025.02.010

* Corresponding Author Email: *mohammad.jalilinik@gmail.com*
s.mozhdehmirzaei@gmail.com
afsbahrami91@yahoo.com

INTRODUCTION

Glioblastoma is a common primary brain tumor that is classified into six groups. Among them, glioblastoma (GBM) is the most aggressive, accounting for about 50% of brain tumors. Although chemotherapy, radiotherapy, and surgical methods are commonly employed, patient survival remains poor because of drug resistance and the nature of the blood-brain barrier (BBB) that results in insufficient accumulated dose in the tumor site and reduces the therapeutic efficiency [1, 2]. Hence, new strategies are required to improve therapeutic outcomes. Recently, nanotechnology has been used in the manipulation of materials at the nanoscale to control their size and physical and chemical properties. Nanoparticles (NPs) have attracted attention for cancer therapy and drug delivery to overcome limitations because of their high surface area, small size, and functionalized groups on their surface, and have shown side effects reduction and improved therapy efficiency [3, 4]. Among metallic NPs, zinc oxide nanoparticles (ZnO) have revealed great potential in cancer treatments due to biocompatibility and selective toxicity against cancerous cells by releasing Zn^{2+} ions and generating ROS that leads to apoptosis and cell death [5, 6]. Moreover, the incorporation of different metal ions can alter the physical and chemical characteristics where ZnO was doped by cerium and silver ions, and results showed selective and significant toxicity against cancer cells as well as great photocatalytic activity. Also, Al-doped ZnO showed cytotoxicity against broad cancer cells such as colon, lung, breast, and liver, and antibacterial activity [7-9]. Herein, in this study, cerium and silver were used as dopants because of their prooxidant activities and toxicity effects [10, 11]. Other reports showed incorporation of metal ions as dopants enhances anticancer effects and biocompatibility of ZnO nanoparticles. When copper, cerium, and silver were doped ZnO NPs showed higher toxicity against cancer cells compared to pure ZnO. *Hannachi et al,* were showed the anticancer effects of ZnO enhanced after co-doping ZnO with Ce and ytterbium. [12-14]. There are different physical and chemical approaches for the synthesis of ZnO, including hydrothermal, co-precipitation, sol-gel, and flame combustion; however, their usage is limited due to toxic precursors and cause toxic effects. Plant-based synthesis of ZnO offers a sustainable, economical, and environmentally friendly route. The bioactive compounds present in plant extracts, including phenols, alkaloids, and terpenoid, sserve dual roles as reducing and stabilizing (capping) agents [15, 16]. The *Ziziphora tenuior* L. (Lamiaceae) is a traditional medicine widespread plant around Iran and has been used against various diseases. This plant extract contains pulegone, menthone, thymol, and piperitenon, which provide essential groups for reducing and stabilizing nanoparticles [17]. Nanoparticles can be synthesized through chemical approaches; however, the use of chemical reducing agents poses potential hazards to both the environment and living systems [18]. Hence, the green synthesis of Ce-Ag@ZnO was chosen with *Ziziphora tenuior* L. (Lamiaceae) serving as stablizer due to its unique phytochemical profile and documented bioactivities that are particularly advantageous for anticancer applications. Extracts from *Ziziphora* species are rich in polyphenols, flavonoids, and terpenoids, which assist as highly effective reducing and stabilizing agents during nanoparticle synthesis, preventing aggregation and ensuring uniform morphology [19, 20]. Previous studies have demonstrated the effectiveness of *Ziziphora tenuior* L. in reducing Ag^{+} ions, and confirmed its role in influencing the size, morphology, and antibacterial properties of silver NPs [21, 22]. In addition to Ag nanoparticles, *Ziziphora clinopodioides* leaf extracts have the potential to be used for the synthesis of eco-friendly and economical zinc nanoparticles[23]. However, a study by Hazrati et al showed that *Ziziphora tenuior* has higher antioxidant and reducing power compared to Ziziphora clinopodioides [24]. Therefore, *Ziziphora tenuior* was selected for green synthesis. Here in this study, cerium (Ce) and silver (Ag) were used as dopants to enhance the anticancer efficacy of ZnO. We decided to extend the reaction time and reduce the temperature to decrease and control the size of NPs. In addition, Ziziphora tenuior L. extract acted as a reducer and capping agent to avoid aggregation of NPs. Then their properties and structure were characterized by UV-Vis, XRD, FTIR, and FESEM/EDX/mapping. The anticancer effects of the obtained NPs were investigated against GBM cells (U251 and U87) and normal cells (HFF). To our knowledge, it is the first time that an extract of *Ziziphora tenuior* L. was used for green synthesis of Ce-Ag@ZnO, and their anticancer effects were evaluated on GBM cells.

MATERIALS AND METHODS

Chemicals and reagents

The *Ziziphora tenuior* L. plants were collected from Zoshk village in Razavi Khorasan Province, Iran. Cerium nitrate hexahydrate ($Ce(NO_3)_3 \cdot 6H_2O$, 99.5%), Zinc oxide hexahydrate ($Zn(NO_3)_2.6H_2O$), and silver nitrate ($AgNO_3$, 99%) were bought from Sigma and Merck companies. DMEM-HG, DMEM-F12, along with penicillin-streptomycin, FBS, and trypsin-EDTA were sourced from Gibco (Grand Island, NY, USA). The malignant glioblastoma cells (U87 and U251 cell lines) and normal Human Foreskin Fibroblast cells (HFF cell lines) were supplied by Iran's National Cell Bank at the Pasteur Institute in Tehran, Iran. Assays were performed using a dichloro-dihydro-fluorescein diacetate (DCFDA/H2DCFDA) cellular reactive oxygen species detection kit (Abcam, Cambridge, UK) and Annexin V-FITC assay kits (Cayman Chemical, Michigan, MI, USA). All other chemicals were obtained from Sigma-Aldrich (St. Louis, MO, USA).

Preparation of plant extract

The plant extract was obtained using a modified Sedaghat method [25]. Leaves of *Ziziphora tenuior* L. were collected, thoroughly washed three times to remove soil particles, and dried in the dark at room temperature for 48 h. Subsequently, 2.0 g of the dried leaves was mixed with 150 mL of distilled water and stirred for 2 h at 60 °C. The resulting solution was filtered and stored at 4 °C for further nanoparticle synthesis.

Green synthesis of ZnO and Ce-Ag@ZnO

Firstly, the 3.0 g of $Zn(NO_3)_2.6H_2O$, 0.025 g of $AgNO_3$, and 0.065 g of $Ce(NO_3)_3 \cdot 6H_2O$ were dissolved in 50 mL of water separately. Then, $Ce(NO_3)_3$ and $AgNO_3$ were added gradually into $Zn(NO_3)_2$ under stirring. Following, 30 mL of plant extract was added dropwise and kept under stirring for 18 h at 60 ℃. The obtained mixture was freeze-dried for 24 h and later calcinated at 400 ℃ for 2 h, which resulted in yellow (ZnO) and brown powder (Ce-Ag@ZnO). The same procedure was done for the synthesis of pure ZnO, except that $Ce(NO_3)_3$ and $AgNO_3$ were not added to the ZnO.

Characterization

The UV-Vis spectra of NPs in the form of solution were calculated in the range of 200 to 800 nm by a UV-Vis spectrophotometer (Shimadzu-1800-Japan) at room temperature using water for baseline calibration to analyze the optical properties and band gap of synthesized ZnO and Ce-Ag@ZnO. To characterize the morphology, particle size, and distribution of NPs, FESEM/PSA (MIRA 3-TESCAN, Czech) was employed. ImageJ software was used for particle size analysis based on FESEM images. EDX/mapping was used to determine the weight percentage and distribution of elements. The crystalline structure and crystalline size were investigated by XRD (2θ=10-80^0, Cu Kα= 1.541 Å, Philips). The FTIR was used for the determination of functional groups on the surface of NPs (Shimadzu-8400). The results of these characterization techniques give comprehensive information about the optical, morphological and structural properties of NPs and prospective applications.

Cell Culture and Viability

Cell viability was assessed using an MTT assay on U87, U251, and HFF cell lines. Briefly, cells were seeded in 96-well plates at a density of 1.5×10^4 cells per well in DMEM-HG medium supplemented with 10% FBS and 1% non-essential amino acids (NEA), followed by overnight incubation at 37 °C in a 5% CO_2 atmosphere. The cells were then exposed to different Ce-Ag@ZnO concentrations (0-1000 µg/ml) for 24 to 48 h. Afterward, each well was filled with MTT (5 mg/ml) and incubated for 3 h. After dissolving the formazan crystals in DMSO, an Epoch ELISA reader was utilized to measure absorbance at 570 nm. The GraphPad Prism software was used to determine IC_{50} values.

Annexin V-FITC PI Double Staining Assay

Apoptosis and necrosis induction by Ce-Ag@ZnO in U87 and U251 cells were assessed using an Annexin V-FITC/ PI staining kit. Cells were seeded in 12-well plates at a density of 3×10^5 cells per well and treated with Ce-Ag@ZnO for 24 hours (U87: 20 and 40 µg/mL; U251: 23 and 46 µg/mL). Following treatment, cells were washed with 1× binding buffer, centrifuged, and stained with Annexin V-FITC and PI in the dark for 10 minutes at room temperature. Cell populations (viable, early apoptotic, late apoptotic, and necrotic) were quantified immediately using a BD FACSCalibur flow cytometer (Becton Dickinson, USA) and analyzed with FlowJo software (FlowJo, USA).

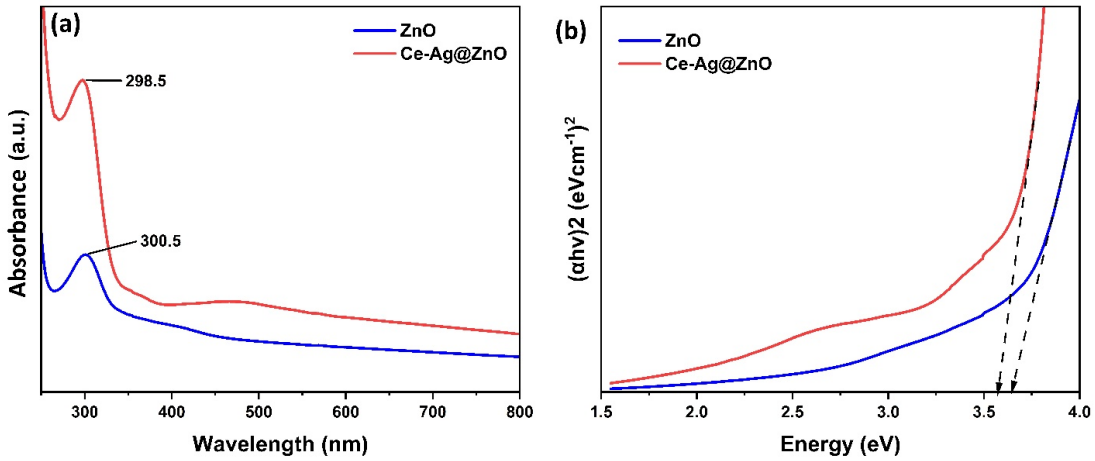

Fig. 1. The UV-Vis spectra of ZnO and Ce-Ag@ZnO demonstrated the following: (a) Maximum absorbance occurred at approximately 296 nm and 300 nm, respectively. (b) The band gap was observed at 3.65 eV and 3.57 eV, respectively.

Measurement of Reactive Oxygen Species (ROS) Generation

Intracellular ROS levels in U87 and U251 cells following Ce-Ag@ZnO exposure were quantified using the H_2DCFDA assay. Cells were seeded in 96-well black plates at a density of 2.5×10^4 cells per well and incubated overnight. After washing, the cells were loaded with 25 µM H_2DCFDA for 45 minutes. Subsequently, cells were rinsed with 1X buffer and treated for 4 hours with Ce-Ag@ZnO (at IC_{50} concentrations of 20 and 40 µg/mL for U87 and 23 and 46 µg/mL for U251) or with 100 µM tert-butyl hydroperoxide (TBHP) as a positive control. Fluorescence intensity (Ex/Em: 485/535 nm) was measured using a Victor X5 microplate reader. All experiments were performed in triplicate.

Statistical Analysis

All data are expressed as mean ± standard deviation. Statistical analyses were performed using GraphPad Prism® version 8.2.1. For multiple comparisons, the Kruskal-Wallis test was applied, followed by Dunn's post hoc test for pairwise comparisons. A p-value of less than 0.05 was considered statistically significant.

RESULTS

UV-Vis spectra

The results of UV-Vis spectra of ZnO and Ce-Ag@ZnO (**Fig. 1**) showed maximum absorbance at around 300 and 302 nm, respectively. The absorption peak of ZnO depends on the size and shape of NPs [26]. When Ce and Ag are added to ZnO, they can induce defects in the grain size and structure of the NPs, creating new localized energy states within the band gap. These changes can lead to an increase in absorbance intensity. Additionally, oxygen deficiency in the ZnO structure can introduce defect energy levels, which can act as electron donors or acceptors, enhancing light absorption. [27, 28]. The Tuac equation (eq1) [29] was used for the calculation of the band gap of ZnO and Ce-Ag@ZnO. The band gap of ZnO decreased from 3.65 to 3.57 eV after doping.

$$(\alpha h\upsilon)^n = \acute{A}\left(h\upsilon - E_g\right) \quad (1)$$

The direct band gap was calculated, so in the Tuac equation, n is 2, A is a constant, and E_g and α are the band gap and absorption coefficient, respectively.

FTIR

The FTIR spectra of ZnO and Ce-Ag@ZnO are presented, ranging from 400 to 4000 cm^{-1} in **Fig. 2**. The results show the characteristic band of metal oxide at 488, which confirms the presence of Zn-O bond and formation of ZnO NPs. A wide band at 3470 cm^{-1} is associated with hydroxyl groups and bands at 1634 and 1478 cm^{-1} appeared because of C=O and C=C groups of phenolic and flavonoid compounds. The bands at 1384,1160, and 1025 cm^{-1} are scribed to C-H groups of alkaline and C-O-C groups [23]. These bands are related to plant extract and imply that it contains phenolic, flavonoid, and carboxylic groups which had a significant role

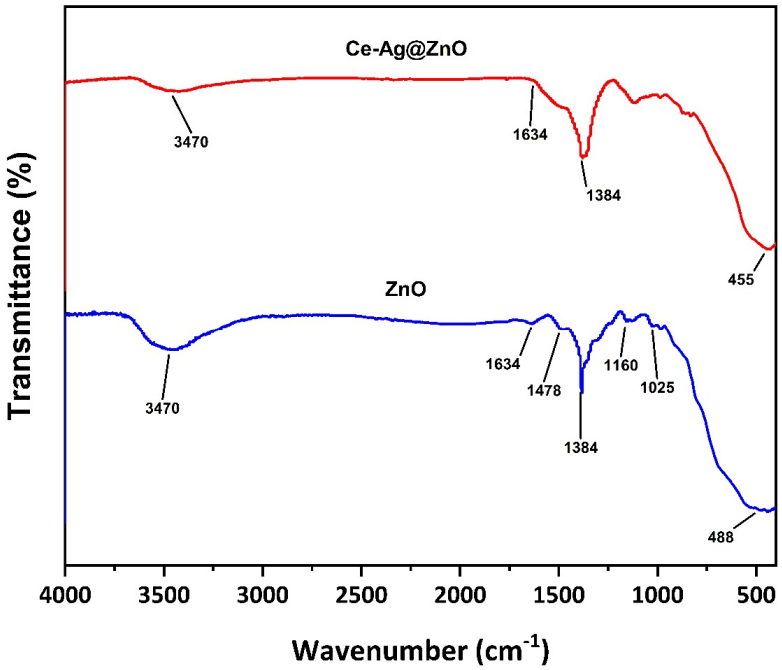

Fig. 2. Fourier-transform infrared (FTIR) spectroscopy was employed to characterize the functional groups of the synthesized nanoparticles. (a) The spectrum for pure ZnO exhibited a band at 488 cm^{-1}, corresponding to the Zn-O stretching vibration. (b) In the Ce-Ag@ZnO spectrum, this peak shifted to a lower wavenumber (455 cm^{-1}), suggesting structural modification due to the incorporation of Ce^{3+} and Ag^{+} ions into the ZnO matrix.

as stabilizers [30]. In the FTIR spectrum of Ce-Ag@ZnO, the intensity of the band at O-H and C-H regions (3470 and 1384 cm^{-1}) decreased and widened, and the band at 1634 cm^{-1} disappeared. Also, a band at 455 cm^{-1} was observed, which indicates the incorporation of Ce and Ag ions into the ZnO structure [31].

XRD

The XRD patterns of nanoparticles presented in **Fig. 3**, show peaks at 31.8°, 34.4°, 36.3°, 47.6°, 56.6°, 62.9°, 66.4°, 68°, and 69.1° indexed with plans (100), (002), (101), (102), (110), (103), (200), (112), and (201), respectively. The results matched with JCPDS No. 01-080-0075 and confirmed the crystallin hexagonal wurtzite structure of ZnO [7]. After doping Ce and incorporation of Ag with ZnO, the peak at the highest angle slightly shifted which may be due replacement of Ce ions in the ZnO lattice structure [32]. Also, peaks 38° and 44.1° matched to (111) and (020) for the cubic structure of Ag based on JCPD No. 01-087-0717 [33, 34]. The strong characteristic, sharp peaks, and no observation of other peaks indicate the high purity of NPs. The crystalline size of ZnO and Ce-Ag@ZnO is calculated by the Debye Scherrer equation (eq2) [7].

$$D = \frac{K\lambda}{\beta \cos\theta} \quad (2)$$

D, k, and λ are the crystalline size (nm), constant (0.94), and the wavelength (0.154 nm), respectively. The β and θ denote FWHM and degree positioning. The crystallite sizes of ZnO and Ce-Ag@ZnO were determined to be 23.6 nm and 27.5 nm, respectively. The observed increase in size may be attributed to the deposition of Ag on the ZnO surface and the substitution of Ce ions into the ZnO lattice, given the larger ionic radius of Ce compared with Zn.

Morphology and elemental composition of NPs

The FESEM images of ZnO and Ce-Ag@ZnO and particle size histograms (**Fig .4**) demonstrate that ZnO are monodispersed spherical shape nanoparticles with an average size of 28.25 ± 1.67 nm that approve the extract of *Ziziphora tenuior* L. acted very well as a reducer and stabilizer. The Ce-Ag@ZnO is spherical with an average size of 31.77

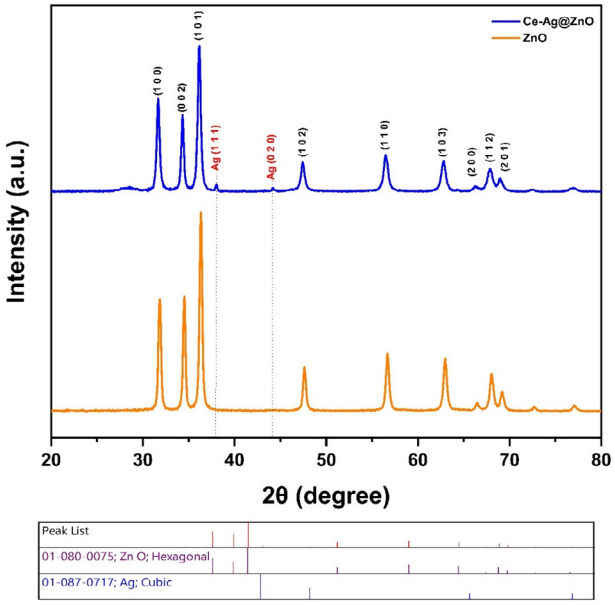

Fig. 3. X-ray diffraction (XRD) analysis was conducted to determine the crystalline phase of the synthesized nanoparticles. (a) The pattern for pure ZnO was consistent with the hexagonal wurtzite structure (JCPDS No. 01-080-0075). (b) The Ce-Ag@ZnO pattern retained the characteristic ZnO peaks but also exhibited additional diffraction peaks corresponding to metallic silver (JCPDS No. 01-087-0717), validating the incorporation of Ag into the composite.

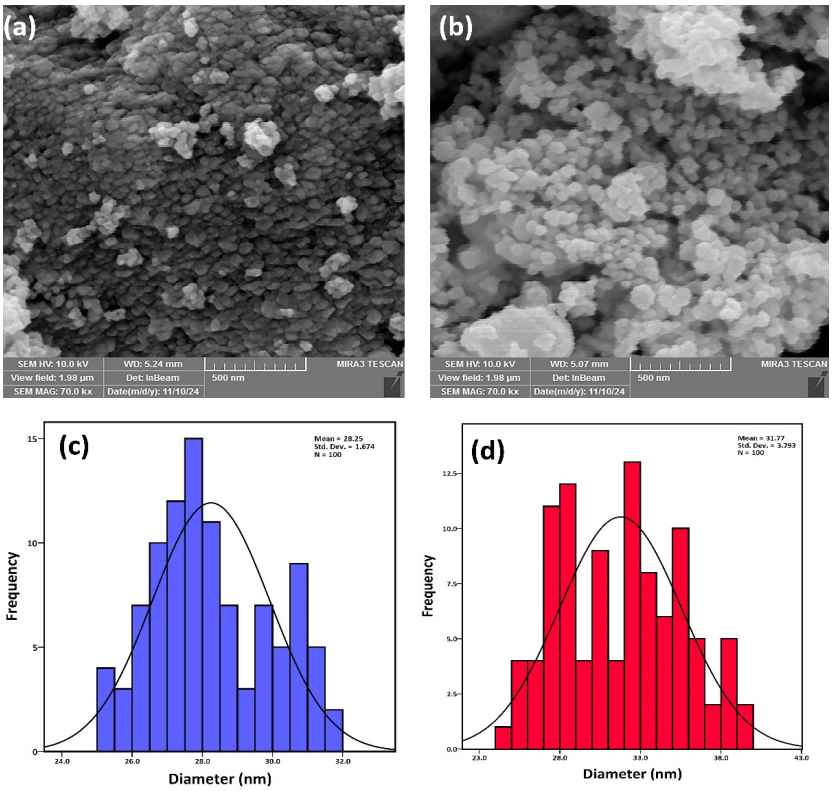

Fig. 4. FESEM analysis was employed to characterize the morphology and size of the synthesized nanoparticles. (a, b) The micrographs demonstrated that both ZnO and Ce-Ag@ZnO consist of spherical particles at the nanoscale. (c, d) Quantitative analysis showed a slight increase in the average particle size from 28 nm for pure ZnO to 31 nm for the Ce-Ag@ZnO composite. This increase in size is consistent with the successful formation of a Ce-Ag co-doped structure.

± 3.7 nm which confirms crystalline size resulting from XRD. These results indicate that after doping, the size of nanoparticles got a little larger which is in agreement with other studies. Other reports showed that the size of ZnO increased after doping with Ag and Ce [7]. The mapping and EDX results (**Fig. 5**) confirm that Ce-Ag@ZnO is composed uniformly of O, Zn, Ce, and Ag with a weight percentage of 33.5, 61.25, 4.61, and 0.78% respectively. The low percentage weight of Ag and Ce is because of the low amount of them used as dopants. The EDX of ZnO shows high purity of ZnO with the existence of only Zn and O with weight percentages of 57.6 and 42.4%. A comparison of EDX results of Ce-Ag@ZnO and ZnO indicates that Ag and Ce doped to ZnO successfully with high purity.

Anticancer

MTT assay

The cytotoxicity of Ce-Ag@ZnO against malignant U251 and U87 GBM cancer cells was examined using an MTT assay kit. The results show (**Fig. 6**) that Ce-Ag@ZnO reduced the viability of GBM cancer cells (U87 and U251 cell lines), with IC_{50} values of 40.56 and 45.44 µg/mL after 24 h. Furthermore, the IC_{50} values for U87 and U251 cell lines after 48 h were evaluated to be 29.54 and 38.73 µg/mL, respectively, showing a dose and time-dependent suppression of cell growth by Ce-Ag@ZnO (**Table 1**).

Normal HFF cells

To evaluate the selectivity of Ce-Ag@ZnO, its effects on normal human foreskin fibroblast (HFF) cells were investigated. Microscopic examination (Fig. 6) showed that even at a high concentration corresponding to the IC_{50}, HFF cells exhibited only minor signs of cytotoxicity, including slight shrinkage and detachment. This contrasts sharply with the pronounced effects observed in malignant U87 and U251 cells, indicating a favorable selective toxicity. The high IC_{50} value of 127.8 µg/mL quantitatively substantiates the low cytotoxicity of Ce-Ag@ZnO in normal cells.

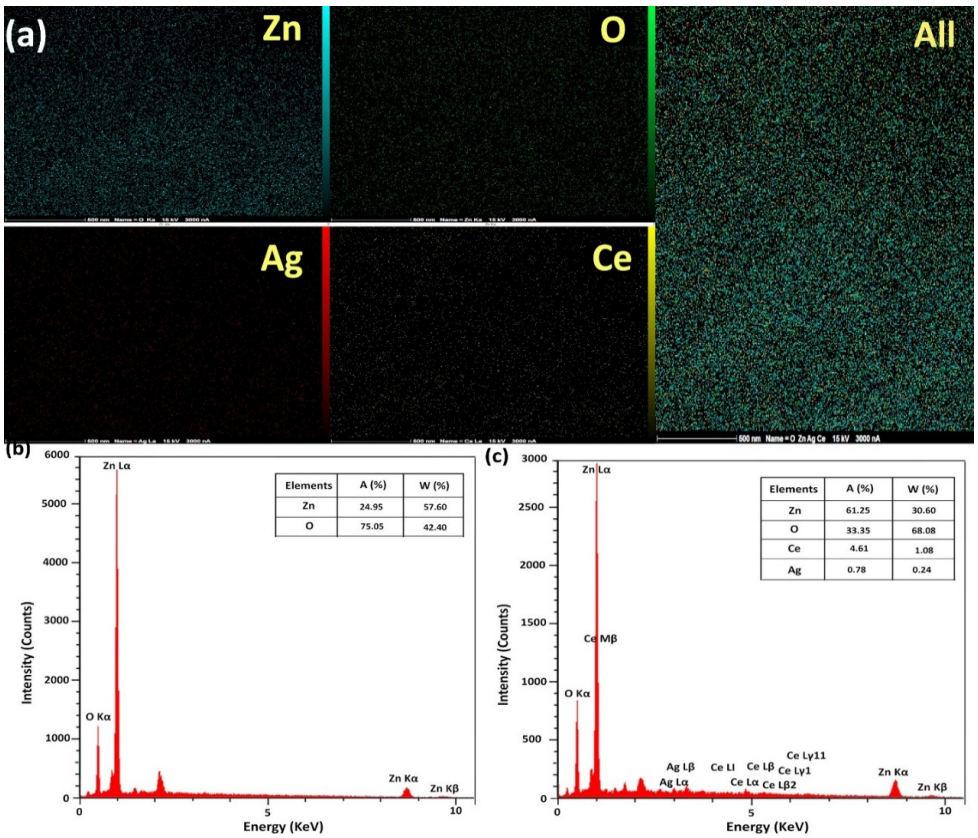

Fig. 5. The mapping and EDX analysis of Ce-Ag@ZnO and ZnO revealed the following: (a) Validation of the primary elements in Ce-Ag@ZnO. (b) The percentages of Zn and O in the ZnO nanoparticle structure were 57.6% and 42.4%, respectively. (c) The percentages of O, Zn, Ce, and Ag in the Ce-Ag@ZnO structure were 33.5%, 61.25%, 4.61%, and 0.78%, respectively

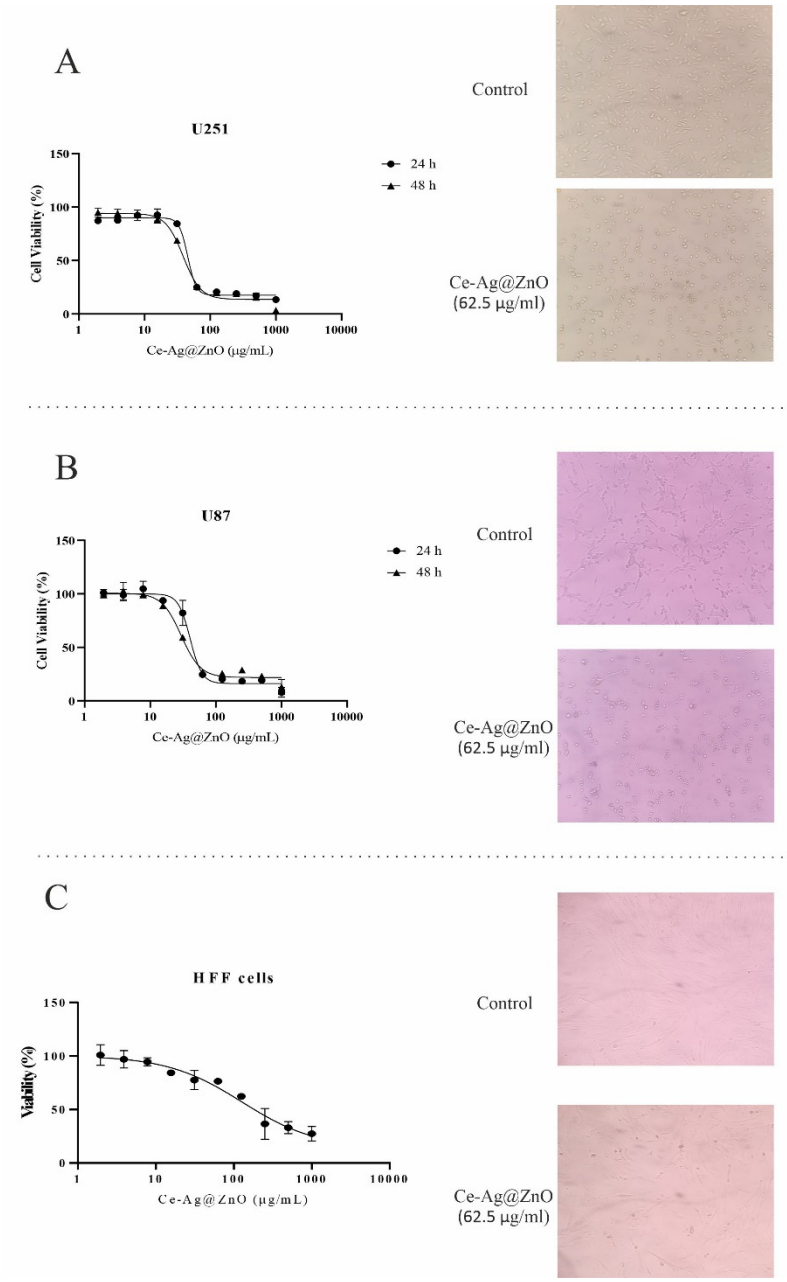

Fig. 6. Evaluating the viability and microscopic images of (A) U251 and (B) U87 GBM and (C) HFF cells following treatment with Ce-Ag@ZnO for 24 and 48 h using MTT assay. Data are expressed as Mean ± SD.

Apoptosis assay

To investigate the pro-apoptotic effects of Ce-Ag@ZnO, U87 and U251 glioma cells were analyzed by flow cytometry following Annexin V-FITC/PI staining. The results (Fig. 7) indicate that Ce-Ag@ZnO treatment induced apoptosis in a dose-dependent manner. Specifically, the compound led to a substantial increase in the percentages of cells in both early and late apoptotic stages compared to the control group.

Ce-Ag@ZnO caused a significant dose-dependent ROS generation

To evaluate the contribution of ROS to the cytotoxic effects of Ce-Ag@ZnO, intracellular ROS levels were quantified fluorimetrically after a 4-hour

Table 1. IC_{50} values of Ce-Ag@ZnO after 24 and 48 h for U87 and U251 GBM cells

U87	24 h	40.56 µg/mL
	48 h	29.54 µg/mL
U251	24 h	45.44 µg/mL
	48 h	38.73 µg/mL
HFF	24 h	127.8 µg/mL

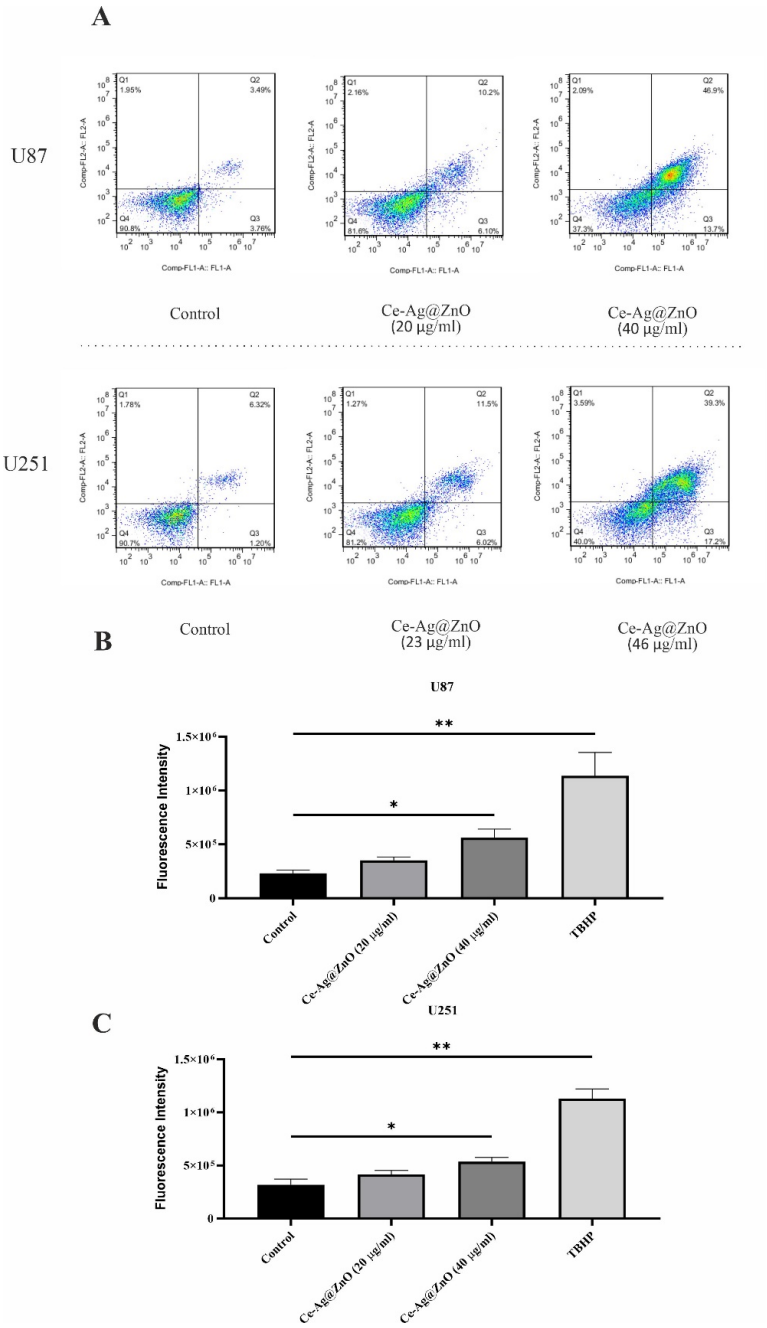

Fig. 7. Analysis of Ce-Ag@ZnO-induced cell death and oxidative stress.(A) Flow cytometric analysis of apoptosis and necrosis via Annexin V-FITC/PI staining in U87 and U251 cells after 24 h. Quadrants: Q4 (viable), Q3 (early apoptotic), Q2 (late apoptotic), Q1 (necrotic). (B, C) Quantification of ROS production using the DCFDA assay in (B) U87 and (C) U251 cells treated for 4 h with Ce-Ag@ZnO; TBHP was used as a positive control. Values represent mean ± SD (n=3 for B and C). *p < 0.05, **p < 0.01 versus control.

incubation. As shown in Fig. 7, Ce-Ag@ZnO induced a significant, concentration-dependent increase in ROS production in both U87 and U251 cells. A similar elevation was observed with TBHP, which was used as a positive control.

DISCUSSION

Despite the efforts for the treatment of glioblastoma multiform (GBM), it is still one of the most challenging health issues due to genetic heterogeneity, the blood-brain barrier, and resistance to therapy [35]. Therefore, nanotechnology was employed to overcome these limitations. Green-synthesized metallic NPs have shown promising applications in anticancer treatments due to their small size, high surface ratio, and biocompatibility. They have been studied as drug delivery vehicles to reduce side effects, minimize environmental effects while maximizing safety in biomedical applications, and enhance anticancer effects for cancer treatments. Using plant extracts for NP synthesis not only reduces toxicity but also enhances biocompatibility, making these NPs suitable for clinical applications [36]. *Ziziphora tenuior* L. is widely grown around Iran and used as a traditional medicine against various diseases. Also, this plant contains various chemical constituents, including Pulegone, menthone, thymol, and piperitenon which provide hydroxyl and carboxyl groups and act as a capping agent and reducer. These components reduce and convert metal ions into zero-valent NPs. Then they adsorb on the surface of NPs prevent aggregation and stabilize NPs. It is important to acknowledge that numerous monoterpenoid compounds, including pulegone, possess anticancer properties [37, 38]. ZnO NPs have gained attraction as an anticancer agent due to their small size, easy synthesis, solubility, high biocompatibility, and ROS production [39]. These NPs are solubilized within the medium or cellular structures, resulting in the release of zinc ions (Zn^{2+}). The released Zn^{2+} triggers a state of zinc-mediated protein activity imbalance and oxidative stress via ROS, which may constitute a potential mechanistic pathway for the cytotoxicity associated with NPs. Considering the selective cytotoxic properties of ZnO-NPs attributable to the enhanced production of ROS within neoplastic cells, these NPs possess the capacity to preferentially target cancerous cells and may be utilized as an anticancer therapeutic agent [29]. It has been found that plant-based preparation of CeO_2-NPs as a drug delivery system significantly promotes anti-tumor potentials [10, 40]. For instance, compared to the temozolomide drug alone, CeO_2-temozolomide exhibited elevated antiproliferative properties, cell cycle arrest, apoptosis, and p53 expression [10]. In a recent study, CeO_2-NPs loaded Urolithin B significantly affected the viability of U87 glioblastoma cells, P53 mRNA expression, and ROS production. Interestingly, CeO_2-Urolithin B presented more considerable anti-GBM effects compared to Urolithin B alone [40]. Silver (Ag) nanoparticles have been shown they have proapoptotic properties and reduce GBM tumor growth significantly [41, 42]. Subsequently, we decided to use Ag to enhance the anticancer effects of ZnO. It should be noted that, as XRD results showed, Ag is incorporated on the surface of ZnO and cannot substitute in the lattice structure of ZnO like Ce. In the present study, Ce-Ag@ZnO decreased the viability of GBM tumor cells (IC_{50} values of 40.56 and 45.44 µg/mL for U87 and U251, respectively, after 24 h). Lower toxicity of Ce-Ag@ZnO towards normal HFF cells demonstrated the highly selective cytotoxicity towards cancer cells while sparing normal cells presents a significant advantage in cancer therapy. We found that Ce-Ag@ZnO at higher doses significantly elevates ROS production in GBM cells (U87 and U251). Another outcome of this study revealed that Ce-Ag@ZnO enhances both early and late apoptosis in a dose-dependent fashion. This effect may be linked to the release of Zn^{2+} ions and the resulting intracellular generation of reactive oxygen species (ROS), suggesting that apoptosis could be initiated through oxidative stress [7, 43]. Mahdizadeh et al. reported that green-synthesized ZnO nanoparticles induced the upregulation of apoptotic markers, including Caspase-3 and Caspase-8, highlighting their role in mediating apoptosis in both in vitro and in vivo breast cancer models [44]. Mansour Kha *et al* synthesized Ce-Ag@ZnO by using *taranjabin* as a stabilizer and investigated their cytotoxicity on breast cancer cells (MDA-MB-231 cell lines) and breast normal cells (MCF-10A cell lines). The results showed doping enhanced the cytotoxicity of pure ZnO against cancer cells, while no significant toxicity on normal cells [7]. Due to the limited research regarding the effects of Z. *tenuior* on GBM cells, this study was initiated to investigate the influence of green-synthesized Ce-Ag@ZnO by using Z. *tenuior* extract on the proliferation of GBM tumor cells. These modifications may induce

apoptotic processes within cellular structures. Our experiment was limited by the use of only two cell lines and a single dose of Ce-Ag@ZnO, which was insufficient to reach a strong conclusion; as such, we are investigating the effects of different concentrations of Ce-Ag@ZnO. Along with the effect of dopants on the structure and chemical characteristics of NPs, the effect of various dopant concentrations requires further investigation.

CONCLUSION

The ZnO and Ce-Ag@ZnO were synthesized via green methods which *Ziziphora tenuior L.* extract was used as a stabilizer and reducer. These NPs were characterized by UV-Vis, XRD, FTIR, FESEM, and EDX/mapping. The FESEM images and EDX/mapping showed ZnO and Ce-Ag@ZnO have homogenously small sizes of 28.25 ± 1.67 and 31.77 ± 3.7 nm, and elements distribute uniformly. UV-Vis, XRD, and FTIR confirm crystalline structure and incorporation of Ce and Ag into ZnO and the successful synthesis of Ce-Ag@ZnO. Also, this modification showed significant selective anticancer activity against GBM. These NPs constitute an innovative and promising strategy in the persistent struggle against GBM. Through a multifaceted mechanism of action that centers on mediating apoptotic responses while concurrently reducing systemic toxicity, these NPs underscore the prospective role of nanotechnology in forthcoming cancer treatment modalities. By further investigating their synergistic effects and optimizing their formulations, these NPs could pave the way for more effective and targeted cancer therapies. Future research will assist in clarifying their roles and promote the therapeutic landscape for treating resistant forms of cancer like GBM. The translational capacity of these NPs may indicate a noteworthy progression in ameliorating GBM prognosis and patient outcomes, emphasizing the vital convergence of nanotechnology, plant biochemistry, and oncological therapeutics.

ACKNOWLEDGMENT

We would like to thank the Clinical Research Development Unit, Imam Reza Hospital, Mashhad University of Medical Sciences, for their assistance in this manuscript.

AUTHOR CONTRIBUTIONS

M.S, S.S.A, O.B: Methodology, Investigation, M.H: Investigation, Software, Writing – original draft, M.P, S.A: Formal analysis, Methodology, Writing – review and editing, M.J-N, S.M.M, A.B: Conceptualization, Data curation, Supervision, Writing – review and editing

CONFLICT OF INTEREST

The authors declare that there is no conflict of interest.

FUNDING

This study was supported by Mashhad University of Medical Sciences (Grant number: 4030958)

DATA AVAILABILITY

Afsane Bahrami. Anticancer activity of green synthesized silver and cerium double-doped zinc oxide nanoparticles by Ziziphora tenuior L. extract against glioblastoma via mediating apoptotic effects[DS/OL]. V1. Science Data Bank, 2025[2025-06-09]. https://cstr.cn/31253.11.sciencedb.25358. CSTR:31253.11.sciencedb.25358.

REFERENCES

1. Ghaznavi H, Afzalipour R, Khoei S, Sargazi S, Shirvalilou S, Sheervalilou R, et al. New insights into targeted therapy of glioblastoma using smart nanoparticles. Cancer Cell Int. 2024;24(1):160. https://doi.org/10.1186/s12935-024-03331-3
2. Rodà F, Caraffi R, Picciolini S, Tosi G, Vandelli MA, Ruozi B, et al. Recent Advances on Surface-Modified GBM Targeted Nanoparticles: Targeting Strategies and Surface Characterization. Int J Mol Sci. 2023;24(3):2496. https://doi.org/10.3390/ijms24032496
3. Al-Thani AN, Jan AG, Abbas M, Geetha M, Sadasivuni KK. Nanoparticles in cancer theragnostic and drug delivery: A comprehensive review. Life Sci. 2024;352:122899. https://doi.org/10.1016/j.lfs.2024.122899
4. Yao Y, Zhou Y, Liu L, Xu Y, Chen Q, Wang Y, et al. Nanoparticle-Based Drug Delivery in Cancer Therapy and Its Role in Overcoming Drug Resistance. Front Mol Biosci. 2020;7:193. https://doi.org/10.3389/fmolb.2020.00193
5. Akhtar MJ, Ahamed M, Kumar S, Khan MAM, Ahmad J, Alrokayan SA. Zinc oxide nanoparticles selectively induce apoptosis in human cancer cells through reactive oxygen species. Int J Nanomedicine. 2012;7:845-57. https://doi.org/10.2147/IJN.S29129
6. Gomaa S, Nassef M, Tabl G, Zaki S, Abdel-Ghany A. Doxorubicin and folic acid-loaded zinc oxide nanoparticles-based combined anti-tumor and anti-inflammatory approach for enhanced anti-cancer therapy. BMC Cancer. 2024;24(1):34. https://doi.org/10.1186/s12885-023-11714-4
7. Al-Enazi NM, Alsamhary K, Kha M, Ameen F. In vitro anticancer and antibacterial performance of biosynthesized Ag and Ce co-doped ZnO NPs. Bioprocess Biosyst Eng. 2023;46(1):89-103. https://doi.org/10.1007/s00449-022-02815-8
8. Asif M, Fakhar-e-Alam M, Tahir M, Jamil F, Sardar H, Rehman J, et al. Synthesis, Characterization, and Evaluation

of the Antimicrobial and Anticancer Activities of Zinc Oxide and Aluminum-Doped Zinc Oxide Nanocomposites. Pharmaceuticals (Basel). 2024;17(3):386. https://doi.org/10.3390/ph17091216
9. Nguyen-Hong YX, Luu TVH, Doan VD. Green synthesis of Ce-doped ZnO nanoparticles using Hedyotis capitellata Leaf extract for efficient photocatalytic degradation of Methyl Orange. Vietnam J Chem. 2021;59(5):648-59. https://doi.org/10.1002/vjch.202100031
10. Foroutan Z, Afshari AR, Sabouri Z, Mostafapour A, Far BF, Jalili-Nik M, et al. Plant-based synthesis of cerium oxide nanoparticles as a drug delivery system in improving the anticancer effects of free temozolomide in glioblastoma (U87) cells. Ceram Int. 2022;48(20):30441-50. https://doi.org/10.1016/j.ceramint.2022.06.322
11. Tunç T. Synthesis and characterization of silver nanoparticles loaded with carboplatin as a potential antimicrobial and cancer therapy. Cancer Nanotechnol. 2024;15(1):2. https://doi.org/10.1186/s12645-023-00243-1
12. Khafaga DSR, Eid MM, Mohamed MH, Abdelmaksoud MDE, Afify M, El-Khawaga AM, et al. Enhanced anticancer activity of silver doped zinc oxide magnetic nanocarrier loaded with sorafenib for hepatocellular carcinoma treatment. Sci Rep. 2024;14(1):15538. https://doi.org/10.1038/s41598-024-65235-6
13. Ghaznavi H, Hajinezhad MR, Hesari Z, Shirvaliloo M, Sargazi S, Shahraki S, et al. Synthesis, characterization, and evaluation of copper-doped zinc oxide nanoparticles anticancer effects: in vitro and in vivo experiments. BMC Cancer. 2025;25(1):37. https://doi.org/10.1186/s12885-024-13398-w
14. Hannachi E, Khan FA, Slimani Y, Rehman S, Trabelsi Z, Akhtar S, et al. In Vitro Antimicrobial and Anticancer Peculiarities of Ytterbium and Cerium Co-Doped Zinc Oxide Nanoparticles. Biology (Basel). 2022;11(12):1836. https://doi.org/10.3390/biology11121836
15. Ogunyemi SO, Abdallah Y, Zhang M, Fouad H, Hong X, Ibrahim E, et al. Green synthesis of zinc oxide nanoparticles using different plant extracts and their antibacterial activity against Xanthomonas oryzae pv. oryzae. Artif Cells Nanomed Biotechnol. 2019;47(1):341-52. https://doi.org/10.1080/21691401.2018.1557671
16. Zhou XQ, Hayat Z, Zhang DD, Li MY, Hu S, Wu Q, et al. Zinc Oxide Nanoparticles: Synthesis, Characterization, Modification, and Applications in Food and Agriculture. Processes. 2023;11(4):1193. https://doi.org/10.3390/pr11041193
17. Ghassemi N, Ghanadian M, Ghaemmaghami L, Kiani H. Development of a Validated HPLC/Photodiode Array Method for the Determination of Isomenthone in the Aerial Parts of Ziziphora tenuior L. Jundishapur J Nat Pharm Prod. 2013;8(4):180-6. https://doi.org/10.17795/jjnpp-12504
18. Hussain I, Singh NB, Singh A, Singh H, Singh SC. Green synthesis of nanoparticles and its potential application. Biotechnol Lett. 2016;38(4):545-60. https://doi.org/10.1007/s10529-015-2026-7
19. Rafique A, Amjad F, Janjua MRSA, Naqvi SAR, Hassan SU, Abdullah H, et al. Chia seed-mediated fabrication of ZnO/Ag/Ag2O nanocomposites: structural, antioxidant, anticancer, and wound healing studies. Front Chem. 2024;12:1405385. https://doi.org/10.3389/fchem.2024.1405385
20. Sedaghat S. Green biosynthesis of Silver-Montmorillonite Nanocomposite using Water Extract of Ziziphora Tenuior L. Curr Nanosci. 2016;12(1):79-82. https://doi.org/10.2174/1573413711666150812010229
21. Jagtap UB, Bapat VA. Green synthesis of silver nanoparticles using Artocarpus heterophyllus Lam. seed extract and its antibacterial activity. Ind Crops Prod. 2013;46:132-7. https://doi.org/10.1016/j.indcrop.2013.01.019
22. Nadagouda MN, Hoag G, Collins J, Varma RS. Green Synthesis of Au Nanostructures at Room Temperature Using Biodegradable Plant Surfactants. Cryst Growth Des. 2009;9(11):4979-83. https://doi.org/10.1021/cg9007685
23. Mahdavi B, Saneei S, Qorbani M, Zhaleh M, Zangeneh A, Zangeneh MM, et al. Ziziphora clinopodioides Lam leaves aqueous extract mediated synthesis of zinc nanoparticles and their antibacterial, antifungal, cytotoxicity, antioxidant, and cutaneous wound healing properties under in vitro and in vivo conditions. Appl Organomet Chem. 2019;33(11):e5164. https://doi.org/10.1002/aoc.5164
24. Hazrati S, Govahi M, Sedaghat M, Beyraghdar Kashkooli A. A comparative study of essential oil profile, antibacterial and antioxidant activities of two cultivated Ziziphora species (Z. clinopodioides and Z. tenuior). Ind Crops Prod. 2020;157:112942. https://doi.org/10.1016/j.indcrop.2020.112942
25. Sedaghat S, Afshar P. Green bio-synthesis of silver nanoparticles using Ziziphora tenuior L water extract. J Appl Chem Res. 2016;10(3):9-18.
26. Sánchez-Pérez DM, Flores-Loyola E, Márquez-Guerrero SY, Galindo-Guzman M, Marszalek JE. Green Synthesis and Characterization of Zinc Oxide Nanoparticles Using Larrea tridentata Extract and Their Impact on the In-Vitro Germination and Seedling Growth of Capsicum annuum. Sustainability. 2023;15(14):11264. https://doi.org/10.3390/su15043080
27. Pradeev raj K, Sadaiyandi K, Kennedy A, Sagadevan S, Chowdhury ZZ, Johan MRB, et al. Influence of Mg Doping on ZnO Nanoparticles for Enhanced Photocatalytic Evaluation and Antibacterial Analysis. Nanoscale Res Lett. 2018;13(1):229. https://doi.org/10.1186/s11671-018-2643-x
28. Pratomo U, Fransisca N, Adzani MD, Irkham I, Sulaeman AP, Eddy DR, et al. Doping of rare earth element: The effects in elevated physical and optical properties of ZnO. Talanta Open. 2025;11:100411. https://doi.org/10.1016/j.talo.2025.100411
29. Ekennia AC, Uduagwu DN, Nwaji NN, Oje OO, Emma-Uba CO, Mgbii SI, et al. Green Synthesis of Biogenic Zinc Oxide Nanoflower as Dual Agent for Photodegradation of an Organic Dye and Tyrosinase Inhibitor. J Inorg Organomet Polym Mater. 2021;31(2):886-97. https://doi.org/10.1007/s10904-020-01729-w
30. Pillai AM, Sivasankarapillai VS, Rahdar A, Joseph J, Sadeghfar F, Anuf AR, et al. Green synthesis and characterization of zinc oxide nanoparticles with antibacterial and antifungal activity. J Mol Struct. 2020;1211:128107. https://doi.org/10.1016/j.molstruc.2020.128107
31. Kaningini AG, Azizi S, Sintwa N, Mokalane K, Mohale KC, Mudau FN, et al. Effect of Optimized Precursor Concentration, Temperature, and Doping on Optical Properties of ZnO Nanoparticles Synthesized via a Green Route Using Bush Tea (Athrixia phylicoides DC.) Leaf Extracts. ACS Omega. 2022;7(36):31658-66. https://doi.org/10.1021/acsomega.2c00530

32. Hamidian K, Saberian MR, Miri A, Sharifi F, Sarani M. Doped and un-doped cerium oxide nanoparticles: Biosynthesis, characterization, and cytotoxic study. Ceram Int. 2021;47(10):13895-902. https://doi.org/10.1016/j.ceramint.2021.01.256
33. Kumar R, Umar A, Kumar G, Akhtar MS, Wang Y, Kim SH. Ce-doped ZnO nanoparticles for efficient photocatalytic degradation of direct red-23 dye. Ceram Int. 2015;41(6):7773-82. https://doi.org/10.1016/j.ceramint.2015.02.110
34. Primo JO, Horsth DF, Correa JDS, Das A, Bittencourt C, Umek P, et al. Synthesis and Characterization of Ag/ZnO Nanoparticles for Bacteria Disinfection in Water. Nanomaterials (Basel). 2022;12(20):3674. https://doi.org/10.3390/nano12101764
35. Lei J, Huang Y, Zhao Y, Zhou Z, Mao L, Liu Y. Nanotechnology as a new strategy for the diagnosis and treatment of gliomas. J Cancer. 2024;15(14):4643-55. https://doi.org/10.7150/jca.96859
36. Ahmadi Shadmehri AA, Namvar F. A review on green synthesis, cytotoxicity mechanism and antibacterial activity of Zno-NPs. J Res Appl Basic Med Sci. 2020;6(1):23-31.
37. Andrade LN, Lima TC, Amaral RG, Pessoa CO, Filho MOM, Soares BM, et al. Evaluation of the cytotoxicity of structurally correlated p-menthane derivatives. Molecules. 2015;20(7):13264-80. https://doi.org/10.3390/molecules200713264
38. Pirbalouti AG, Amirkhosravi A, Bordbar F, Hamedi B. Diversity in the chemical composition of essential oils of Ziziphora tenuior as a potential source of pulegone. Chemija. 2013;24(3):234-9. https://doi.org/10.6001/chemija.2013.24.3.9
39. Anjum S, Hashim M, Malik SA, Khan M, Lorenzo JM, Abbasi BH, et al. Recent Advances in Zinc Oxide Nanoparticles (ZnO NPs) for Cancer Diagnosis, Target Drug Delivery, and Treatment. Cancers (Basel). 2021;13(18):4570. https://doi.org/10.3390/cancers13184570
40. Mohammad GRK, Motavalizadehkakhky A, Darroudi M, Zhiani R, Mehrzad J, Afshari AR. Urolithin B loaded in cerium oxide nanoparticles enhances the anti-glioblastoma effects of free urolithin B in vitro. J Trace Elem Med Biol. 2023;78:127186. https://doi.org/10.1016/j.jtemb.2023.127186
41. Santos ICG, de Oliveira ML, Silva RC, Sant'Anna C. Assessment of silver nanoparticles' antitumor effects: Insights into cell number, viability, and morphology of glioblastoma and prostate cancer cells. Toxicol In Vitro. 2024;99:105869. https://doi.org/10.1016/j.tiv.2024.105869
42. Urbańska K, Pająk B, Orzechowski A, Sokołowska J, Grodzik M, Sawosz E, et al. The effect of silver nanoparticles (AgNPs) on proliferation and apoptosis of in ovo cultured glioblastoma multiforme (GBM) cells. Nanoscale Res Lett. 2015;10(1):98. https://doi.org/10.1186/s11671-015-0823-5
43. Vijayakumar G, Boopathi G, Elango M. In vitro cytotoxic efficacy of PEG encapsulated manganese-doped zinc oxide nanoparticles on hepatocellular carcinoma cells. Mater Technol. 2019;34(13):807-17. https://doi.org/10.1080/10667857.2019.1633787
44. Mahdizadeh R, Homayouni-Tabrizi M, Neamati A, Seyedi SMR, Tavakkol Afshari HS. Green synthesized-zinc oxide nanoparticles, the strong apoptosis inducer as an exclusive antitumor agent in murine breast tumor model and human breast cancer cell lines (MCF7). J Cell Biochem. 2019;120(10):17984-93. https://doi.org/10.1002/jcb.29065